

A Stimuli-Responsive Nanocomposite for 3D Anisotropic Cell-Guidance and Magnetic Soft Robotics

Riccardo Tognato, Angela R. Armiento, Valentina Bonfrate, Riccardo Levato, Jos Malda, Mauro Alini, David Eglin, Gabriele Giancane, and Tiziano Serra*

Stimuli-responsive materials have the potential to enable the generation of new bioinspired devices with unique physicochemical properties and cell-instructive ability. Enhancing biocompatibility while simplifying the production methodologies, as well as enabling the creation of complex constructs, i.e., via 3D (bio)printing technologies, remains key challenge in the field. Here, a novel method is presented to biofabricate cellularized anisotropic hybrid hydrogel through a mild and biocompatible process driven by multiple external stimuli: magnetic field, temperature, and light. A low-intensity magnetic field is used to align mosaic iron oxide nanoparticles (IOPs) into filaments with tunable size within a gelatin methacryloyl matrix. Cells seeded on top or embedded within the hydrogel align to the same axes of the IOPs filaments. Furthermore, in 3D, C2C12 skeletal myoblasts differentiate toward myotubes even in the absence of differentiation media. 3D printing of the nanocomposite hydrogel is achieved and creation of complex heterogeneous structures that respond to magnetic field is demonstrated. By combining the advanced, stimuli-responsive hydrogel with the architectural control provided by bioprinting technologies, 3D constructs can also be created that, although inspired by nature, express functionalities beyond those of native tissue, which have important application in soft robotics, bioactuators, and bionic devices.

1. Introduction

Anisotropy of biological tissues is an essential feature associated with their development, functions, and regeneration.^[1,2] To recapitulate in a Petri dish the intrinsic properties of the in vivo milieu, including anisotropy, cells can be embedded in a carefully designed extracellular matrix-like material that provides a heterogeneous assortment of biophysical and biochemical cues. Stimuli-responsive hydrogels represent excellent candidate materials, thanks to their cell scaffolding capabilities and potential for applications in soft robotics, although they intrinsically lack anisotropy.^[3,4] Although extensively used in biological applications, they are prevalently responsive to thermal and pH/osmotic stimuli, and are consequently rather slow or difficult to control.^[5–7] Among the approaches described for the generation of anisotropic hydrogels, Bae et al. used photolithography technologies to pattern nanogroves able to guide the cell orientation on the hydrogel surface.^[8] External electric or magnetic fields have also been used to assemble


linear chains of colloidal particles.^[9] Quick responsivity and hydrogel anisotropy have been achieved by incorporation in pre-hydrogel solutions of magnetic reactive elements, the organization of which is remotely controlled by a low-intensity external magnetic field before gelation occurs.^[10] When immersed in an external static and uniform magnetic field, paramagnetic iron oxide nanoparticles (IOPs) self-assemble in a filamentous structure owing to the dipole–dipole magnetic attraction between IOPs.^[11,12] The high biocompatibility of iron oxide-based nanostructures makes them suitable for many biomedical applications. IOPs have been used as therapeutic compounds,^[13] diagnostic tools,^[14] and biosensors.^[15] Hu et al. reported the fabrication of anisotropic hydrogels via the dispersion of magnetic nanospheres in a solution of monomers, their self-assembly in presence of an external magnetic field, and subsequent immobilization upon polymerization at high temperature ($\approx 50^\circ\text{C}$).^[12] However, this process is not suitable for the simultaneous embedding of cells. Others have reported an injectable anisotropic hydrogel in which superparamagnetic IOPs/poly(lactic-co-glycolic acid) (PLGA)

R. Tognato, Dr. A. R. Armiento, Prof. M. Alini, Dr. D. Eglin, Dr. T. Serra
AO Research Institute Davos
Clavadelerstrasse 8, 7270 Davos Platz, Switzerland
E-mail: tiziano.serra@aofoundation.org

Dr. V. Bonfrate, Dr. G. Giancane
Department of Cultural Heritage
University of Salento
Via D. Birago, 73100 Lecce, Italy

Dr. R. Levato, Prof. J. Malda
Regenerative Medicine Center Utrecht and Department
of Orthopaedics
University Medical Center Utrecht
Heidelberglaan 100, 3584 CX, Utrecht, The Netherlands

Prof. J. Malda
Department of Equine Sciences
Faculty of Veterinary Sciences
Utrecht University
Yalelaan 112, 3584 CM Utrecht, The Netherlands

 The ORCID identification number(s) for the author(s) of this article can be found under <https://doi.org/10.1002/adfm.201804647>.

DOI: 10.1002/adfm.201804647

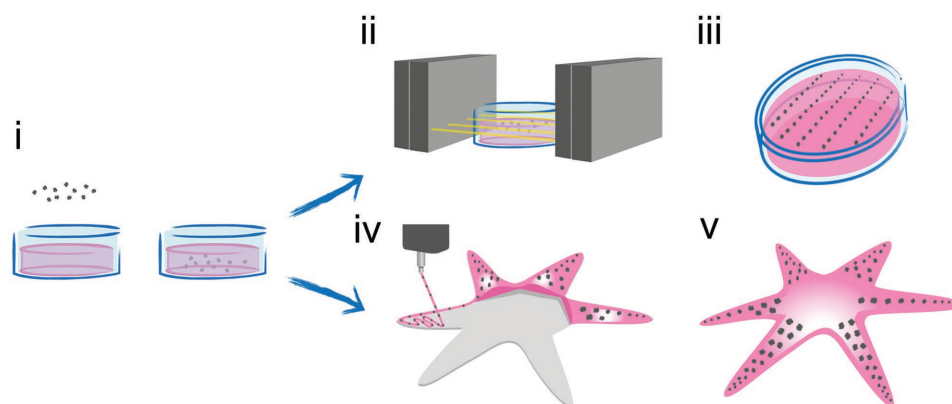


Figure 1. Schematic representation for the anisotropic nanocomposite fabrication and the 3D-printed star-shaped magnetic soft robot. i) IOPs addition to a liquid suspension ($T > 37\text{ }^{\circ}\text{C}$) of G hydrogel precursor. ii) Application of low-intensity magnetic field. iii) Formation of the oriented IOPs filaments while the mixture temperature decreases below melting temperature and final crosslinking via UV-light of the anisotropic nanocomposite. iv) 3D printing of the G/IOPs mixture on a bed of G hydrogels. v) The 3D-printed structure is finally crosslinked by UV-light resulting in a stable star-shaped responsive structure.

electrospun nanofibers were first cut into small fragments with a microtome, and were subsequently dispersed in poly(ethylene glycol) (PEG) prepolymers (20 wt:vol%) before being finally oriented by a low-intensity external magnetic field ($<300\text{ mT}$) prior to curing.^[16] Nerve cells seeded on the surface subsequently aligned parallel to the nanofibers. An interesting responsive hydrogel is methacryloyl gelatin, also known as GelMA (G), which is a temperature responsive and photopolymerizable material.^[17] Conductive G-based hydrogels containing carbon nanotubes (CNT) aligned via dielectrophoresis have also been reported, and tested for cell response seeding immortalized mouse myoblasts (C2C12 cell line) on the 2D surface of the material.^[18,19] Muscle cells maturation was achieved with the application of an electrical field. However, with such approach, the observed cell response may not be solely due to the created anisotropic CNT organization, but also to the polarization gradient of small proteins within the hydrogels due to the dielectrophoresis.^[20] Other limitations of the above reported studies are the use of long and complicated manufacturing processes for the hydrogel network formation^[16] and the potential toxicity of the CNT.^[19,21] Ensuring nontoxicity and biocompatibility of the manufacturing process is a major challenge toward the fabrication of magnetically responsive materials, based on hydrogel and living cells, that could be used for soft robotics, drug delivery, theranostics, and wound healing.^[4,22–24] In this work, we report a novel method to biofabricate cellularized nanocomposite hydrogels endowed with anisotropy, cell-guiding functionalities in 2D and 3D, and rapid, controllable stimuli-responsiveness through temperature, photocrosslinking and a low-intensity magnetic field (Figure 1i–iii). This material is compatible with biofabrication and 3D printing technologies, allowing the fabrication of functional constructs and soft robots (Figure 1iv,v). Thus, on one hand, our approach provides a promising way to create anisotropic 3D cell culture substrates, that we have explored more in detail especially for muscle tissue engineering. On the other hand, we provide a demonstration of the possibility to use our nanocomposite hydrogel as ink for 3D printing, and therefore its potential to create complex, stimuli-responsive 3D structures through a proof-of-concept application for soft robotics.

2. Results

2.1. Synthesis and Characterization of the IOPs

Transmission electron microscopy (TEM) was used to investigate the morphology of the synthesized IOPs. Incorporating PEG in the synthesis process drastically influenced the formation of the nanoparticles, acting as a surfactant (Figure 2a–c). In presence of PEG, rounded IOPs were produced and the nanoparticles assembled in an aggregated form or mosaic structure (Figure 2a,b).^[25] The diameter of mosaic structures showed a bimodal distribution with peaks at 45 and 60 nm (Figure 2a). Figure 2b shows that the single PEG-capped IOPs were spherical with an average diameter of 3 nm. On the contrary, when the PEG was excluded from the synthesis procedure, square-shaped IOPs particles were formed with clear-cut edges (Figure 2c).

Both for IOPs and for PEG-capped IOPs, X-rays diffraction shows that $\gamma\text{-Fe}_2\text{O}_3$ phase is obtained (Figure 2d), indicating that shape and size of the IOPs are influenced by the presence of PEG without affecting the chemical structure and crystalline phase of the synthesized iron oxide-based nanoparticles. The study of the interaction among inorganic nanoparticles and the PEG capping was carried out by means of Raman spectroscopy (Figure 2e,f). As reported in Table S1 in the Supporting Information, it is possible to conclude that the polymer backbone is mainly involved in the IOPs capping and covalent interactions among $\gamma\text{-Fe}_2\text{O}_3$ nanoparticles and the organic moiety can be excluded.

The effect of the capping on the IOPs electrostatic charge was monitored by means of ζ -potential measurements. The electrical charge contained in the proximity of the particles' surface drastically decreased in presence of the capping polymer, changing from -15.6 to -0.9 mV .

2.2. Anisotropic Hydrogels for Cell Culture and Tissue Engineering

2.2.1. Biofabrication and characterization of the 3D constructs

To develop the anisotropic nanocomposite hydrogel, we applied a very low intensity external magnetic field generated with two

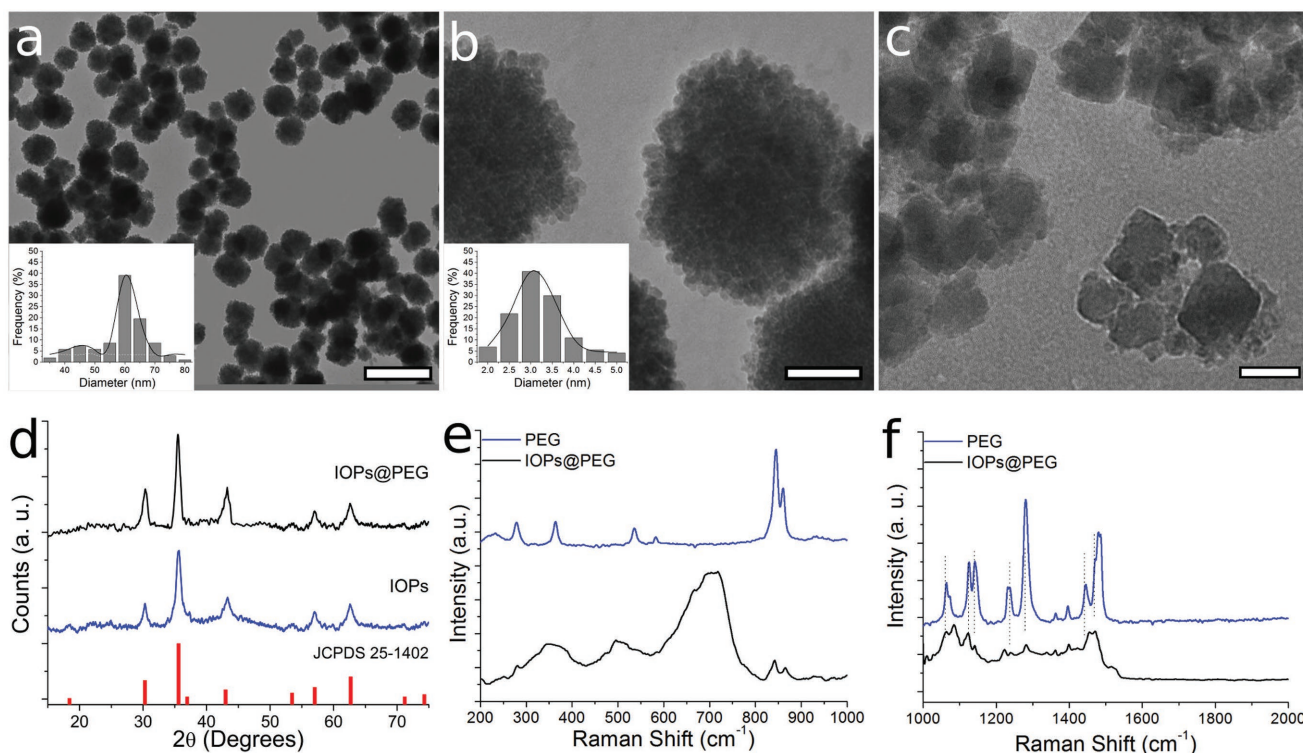


Figure 2. a) TEM image of the PEG-capped iron oxide nanoparticles at low magnification shows the spherical form of the mosaic structures which show a bimodal size distribution centered at 60 and 45 nm (inset). Scale bar = 200 nm. b) Higher magnification TEM image of the mosaic structures shows a size distribution with average diameter of 3 nm (inset). Scale bar = 20 nm. c) TEM images of square-shaped IOPs produced in absence of PEG in the synthetic procedure. Scale bar = 20 nm. d) X-ray diffraction profiles of IOPs and PEG-capped IOPs compared with γ -Fe₂O₃ from reference (JCPDS 25-1402). In boxes e, f) Raman spectra of the synthesized nanostructures are compared.

commercially available and cost-effective permanent magnets (20 mT).^[26] The fabrication process is illustrated in Figure 1i–iii. First, IOPs were added to a liquid solution of G hydrogel precursor ($T > 37$ °C) (i). Second, a low-intensity magnetic field was applied to induce the self-assembly of the IOPs in oriented filaments (ii). Finally, the temperature of the G/IOPs mixture was decreased below the melting temperature stabilizing the self-assembled structures prior to the final chemical crosslinking via UV-light, which resulted in a stable anisotropic nanocomposite hydrogel (iii).

A magnetic field simulation was performed to verify the creation of a static magnetic field with zero gradient lacking IOPs-field force, preventing the IOPs magnetophoretic effect (Figure S3, Supporting Information).^[27] The kinetics of the assembly process demonstrated a rapid growth of the IOPs filaments' length along the field line, with a visible alignment at 1 min (Figure 3a and Figure S4, Supporting Information). The mean length of IOPs filaments continuously increased until 10 min when a plateau was reached (Figure 3a iii). The steep initial decrease in the assembly rate was mainly attributed to the decrease of the IOPs concentration near the growing filaments as the assembly proceeded (Figure 3a iii).^[11] On the other hand, this could also be due to the increment of the drag force induced by the progressive physical gelation of the G prepolymer mixture.^[27,28] Indeed, the temperature-induced gelation led to the stabilization of the IOPs filaments and such anisotropic organization was further stabilized by UV crosslinking. Both

gelation mechanisms did not interfere with the assembled IOPs filaments.^[12]

The analysis of the filament diameter distribution showed a unimodal distribution with a peak around 12.5 μ m, in agreement with the full width at half maximum of the peaks in the iron distribution profile of the aligned samples obtained by energy dispersive X-ray analysis (EDX) (Figure 3d and Figure S6, Supporting Information). The presence of the IOPs in the G prepolymer solution did not influence the temperature- and light-induced gelation time of the hydrogel as is evidenced by the steep increase of G' modulus once the UV-light is applied (Figure S7, Supporting Information). This is possibly due to the absence of a net charge on the surface of the IOPs, and the lack of specific molecular interaction between G and IOPs as shown by the complete overlap of the vibrational bands assigned to G in Fourier-transform infrared spectroscopy (FTIR) spectra of both IOPs-free and IOPs-containing hydrogels (Figure S5, Supporting Information). A UV exposure period of 10 min was chosen for a complete crosslinking (Figure S7, Supporting Information). Different analytical techniques have been used to assess the alignment of the IOPs particles, being this of paramount importance for the generation of anisotropic hydrogel with spatially organized mechanical and chemical cues to direct cells' behavior. Morphological and chemical characterization, conducted by scanning electron microscopy (SEM) coupled with EDX, showed the anisotropic alignment of IOPs throughout the bulk of the G hydrogel when subjected

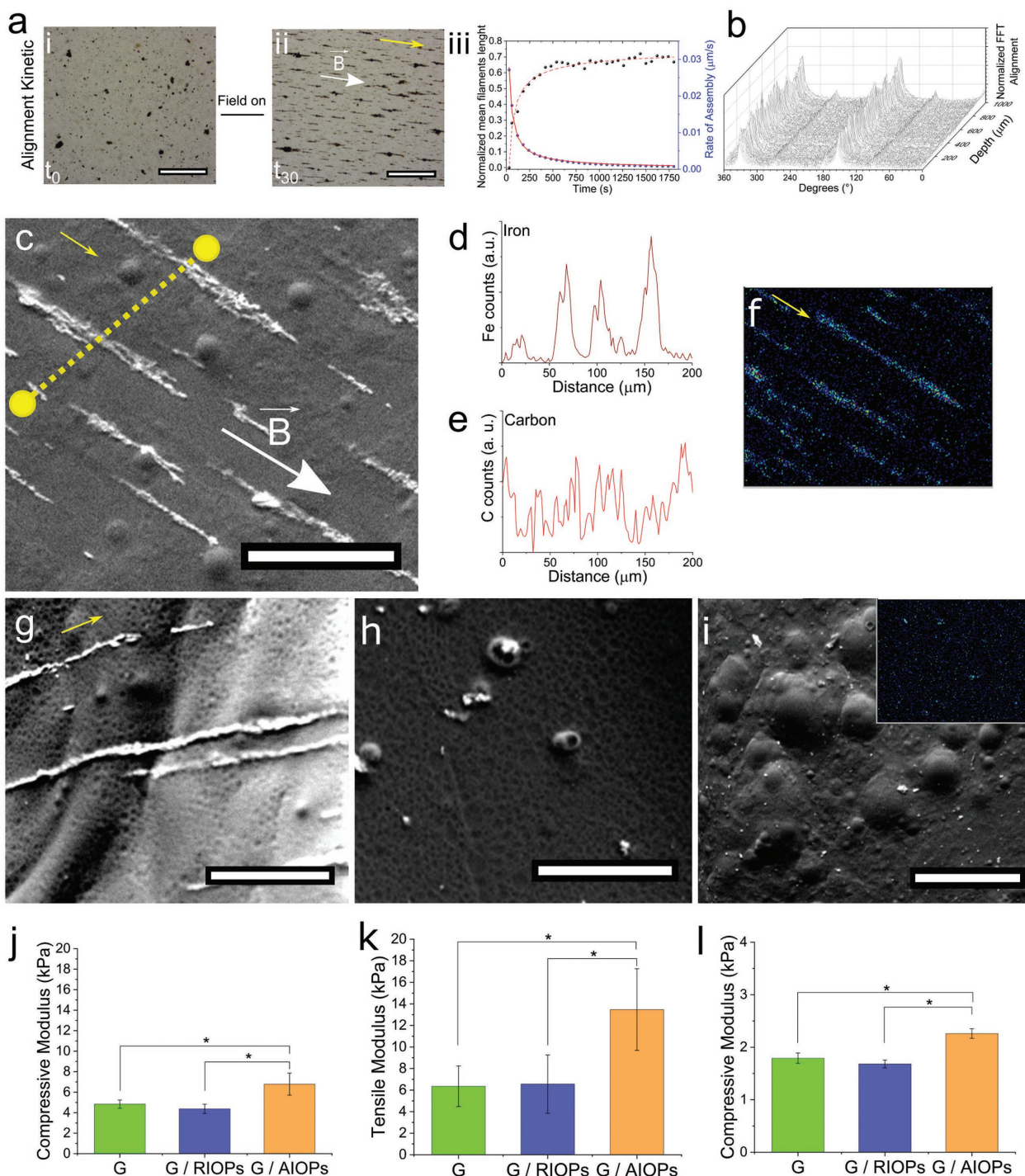


Figure 3. Characterization of the G/IOPs nanocomposite material. a) Time-lapsed picture of the growing filaments of IOPs when subjected to a zero-gradient static magnetic field. Initially, the IOPs are randomly dispersed t_0 . The IOPs pathway growth along the magnetic field lines t_r . Formation kinetic of the elongated IOPs structures mean size growth (black circles) and rate of assembly (blue circles) in a zero-gradient static magnetic field. The data points were determined as the Feret diameter, the solid and the dashed lines represent the fit with a power law function. Scale bar = 500 μm . b) The 2D-FFT analysis of a Z-stack images series, taken for the entire thickness of the G/AIOPs, shows distinct peaks at 170 and 340 degrees indicating the presence of aligned features in the whole 3D hydrogel matrix (Video S1, Supporting Information). c) SEM images of the top surface of the nanocomposite material with IOPs aligned filaments along the external field lines. Scale bar = 200 μm . d) Fe and e) C concentration profile along the ROI. f) Bidimensional Fe atoms surface distribution measured by EDX elemental analysis. g,h) Lateral and cross-section view of the G with the aligned filaments. Scale bar = 50 μm . i) SEM images of the top surface of randomly dispersed G/RIOPs sample, the inset shows the bidimensional Fe atoms surface distribution measured by EDX elemental analysis. Scale bar = 200 μm . j) Compressive modulus, k) tensile modulus, and l) local indentation compressive modulus values of G, G/RIOPs, G/AIOPs. The yellow arrows highlight the direction of alignment of the IOPs filaments. * $P < 0.05$, ** $P < 0.01$, one-way ANOVA with a Tukey post hoc test.

to the magnetic field (Figure 3c–i). This was confirmed by 2D fast Fourier transform analysis (2D-FFT) of bright field images for the entire thickness of the anisotropic nanocomposite G, which showed two peaks of alignment at 165 and 345 degrees (Figure 3b and Video S1, Supporting Information). Introducing aligned structures in G/AIOPs resulted in an overall improvement of mechanical properties of the nanocomposite hydrogels, increasing by 2 kPa the compressive modulus (Figure 3j; Figure S8, Supporting Information), doubling the tensile modulus in the direction parallel to the aligned filaments (Figure 3k), and increasing by 0.5 kPa the stiffness measured by nanoindentation (Figure 3l), when compared to the G/RIOPs and G samples. Similar results in terms of anisotropic mechanical performances due to highly ordered hierarchical nanocomposite structures were also shown by previous works.^[12,29,30]

2.2.2. Cell alignment and differentiation in 2D and 3D

Anisotropic nanocomposites positively influenced the behavior of cells, either seeded on the surface of the hydrogel or embedded in 3D. First, human mesenchymal stem cells (hMSCs) were seeded on top of the nanocomposite hydrogels. On G/RIOPs, hMSCs showed multidirectional spreading with no preferential axis of alignment, as indicated by actin cytoskeleton staining at 24 h (Figure 4a). hMSCs seeded on top of G/AIOPs aligned along the direction of the IOPs filaments as clearly shown by the image at higher magnification (Figure 4b,c). The cells' and the IOPs' orientation measured with 2D-FFT at 4, 24, and 72 h indicated that hMSCs aligned within 24 h on the surface of G/AIOPs (Figure S9, Supporting Information).

Cells' response to the assembly process and hydrogel anisotropy was then studied using C2C12 cells embedded within G/AIOPs, G/RIOPs, and G.

Interestingly, an added benefit of using PEG-capped IOPs, during the cells embedding, was a protective effect on cell viability upon G hydrogel UV-crosslinking. This is shown by the higher number of proliferating cells at day 7 postembedding in G containing IOPs in comparison to the pristine G. In particular, G/RIOPs composites displayed the highest cell amount at day 7, followed by G/AIOPs and then G samples. (Figure 4d,e).

IOPs particles exhibit an absorbance peak in the UV range, which overlaps with the emission wavelength used to crosslink the hydrogel (Figure S1, Supporting Information), and thus may cause a screening effect, reducing the effective irradiation dosage received by the embedded cells. Consequently, the extent of potential damage induced by radicals generated by UV irradiation is lower in samples containing nanoparticles and this may correlate with the higher proliferation rate observed at day 7 (Figure 4d,e). Compared with the anisotropic gels, this beneficial effect is more evident for the hydrogel with randomly dispersed nanoparticles (G/RIOPs), which are distributed homogeneously throughout the gel matrix, possibly providing a bulk screening rather than a local effect.

C2C12 cells encapsulated in 3D hydrogels aligned in the same direction of the IOPs filaments within G/AIOPs within 72 h as assessed by 2D-FFT of the fluorescent images collected at day 1, 3, and 7, postembedding (Figure 4f). Moreover, functionality of

the anisotropic nanocomposite hydrogel was assessed through C2C12 differentiation in mature multinucleated myotubes expressing myosin heavy chain (MyHC). Immunofluorescence images reported in Figure 4g and Figure S10 in the Supporting Information show C2C12 cells encapsulated within 3D hydrogels in the three conditions (G, G/RIOPs, and G/AIOPs) and cultured for the first 7 d in expansion medium and for additional 4 d in either differentiation medium containing 2% horse serum (HS+) or in expansion medium (HS−). When C2C12 cells were embedded in G and cultured in expansion medium for the whole length of the culture, no MyHC staining was observed, indicating the absence of myotube formation. Upon addition of differentiation medium, myosin staining was observed not only in scattered mononuclear cells but also within clusters of cells, suggesting the beginning of multinucleated cell formation. Within G/RIOPs, myosin staining and few multinucleated cells were observed in HS− medium. By adding HS to the G/RIOPs culture, cells started to form small tubular structures. In comparison to G and G/RIOPs, C2C12 cells in G/AIOPs showed enhanced myotube organization in long tubular structures, with a high level of MyHC protein expression (Figures S10 and S11, Supporting Information; Videos S2 and S3, Supporting Information). The myotube organization was further enhanced by the addition of differentiation medium.

By changing the nanoparticle concentration and the distance of the permanent magnets, regulating the magnetostatics fields used for the assembly process, we can easily manipulate the size and length of the nanoparticle filaments, as well as the interfilament spacing. The final nanocomposite architecture is represented by a hydrogel with embedded nanostructured filaments at microscale distances. A number of studies have proved that cells extend both in axial and transversal direction to nano- and microgrooves.^[8,31–33] Nanoparticle filaments could also act as physical barriers guiding cell alignment as shown before.^[32]

Overall, the characteristic dimension of the aligned filaments of nanoparticles within our gels (width of the filament of 12.5 μm and filament-to-filament distance: 50 to 100 μm) was optimized to display values in a range suitable to guide cell alignment.^[31,32] This played an important role in orchestrating a preferential spatial arrangement and anisotropy of the encapsulated myocytes, influencing their cytoskeletal arrangement and eventually their directionality.^[31–33] Moreover, such influence on morphology induced the early maturation of cells toward multinucleated myotubes and may represent a powerful tool to induce muscle tissue organization and morphogenesis.^[1,34,35]

Finally, this technology could potentially be customized to generate anisotropic nanocomposite hydrogels by combining our nanoparticles with different extracellular-matrix like materials besides methacryloyl gelatin, possibly applying different crosslinking mechanisms. For instance, photocrosslinking using visible light initiators^[36–38] could be explored to overcome potential concerns related to UV irradiation.

2.3. 3D-Printed Magnetic Soft Robot

Magneto-responsive biomaterials have raised great interest for a wide array of applications in materials science and engineering.^[10] Alongside providing cell-instructive supports for

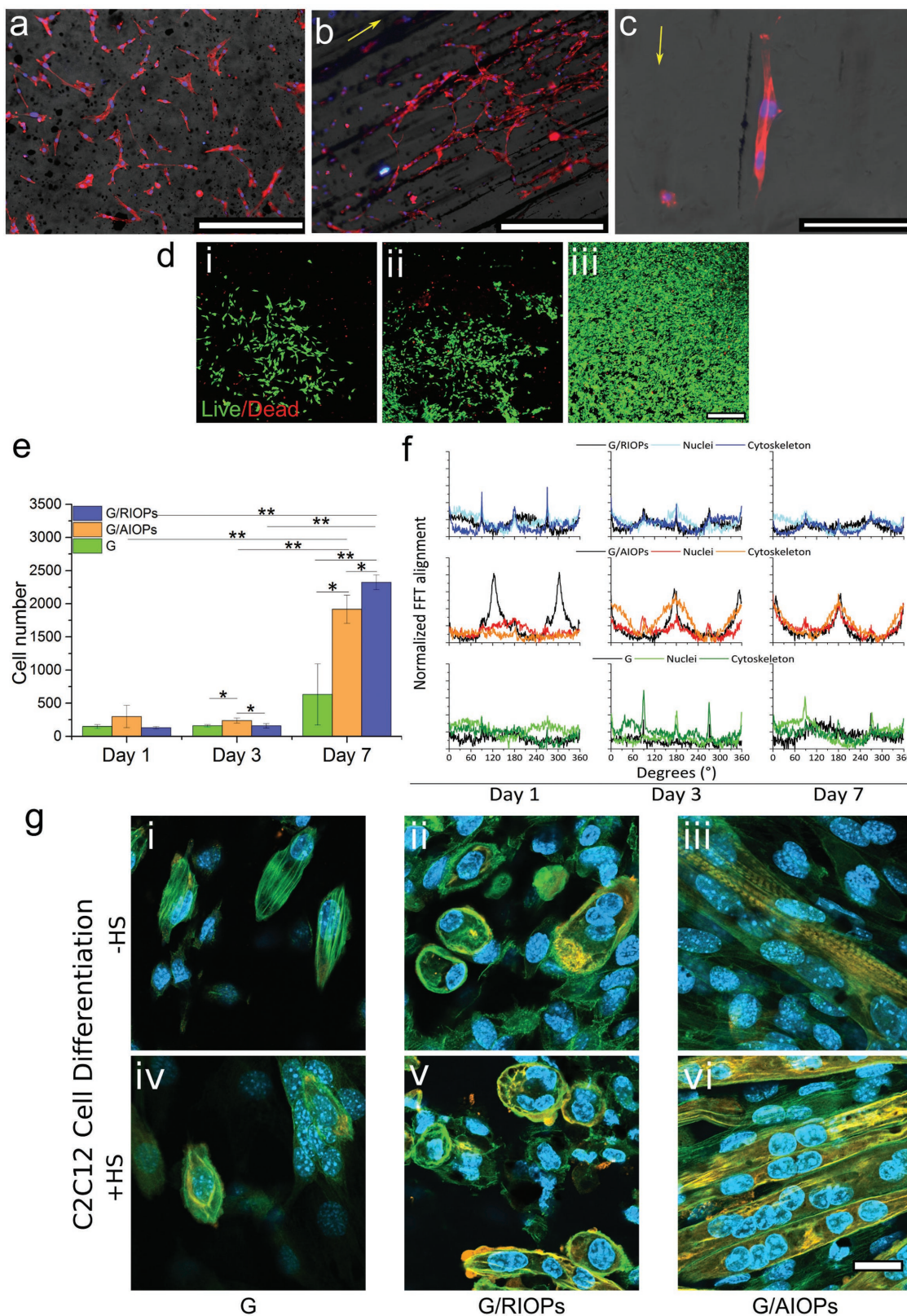


Figure 4. Cells anisotropic nanocomposite material interaction both in 2D and 3D and C2C12 differentiation. a) Fluorescent image of hMSCs seeded on top of G/RIOPs does not show any preferential axis of alignment after 24 h. Scale bar = 400 μm . b) Fluorescent image of hMSCs alignment on top of G/AIOPs after 24 h. Scale bar = 400 μm . c) Higher magnification fluorescent image of hMSC seeded on top of the G/AIOPs which shows the preferential alignment of the cells along the IOPs filaments. Scale bar = 100 μm . The yellow arrows indicate the IOPs filament direction. Actin filaments and nuclei

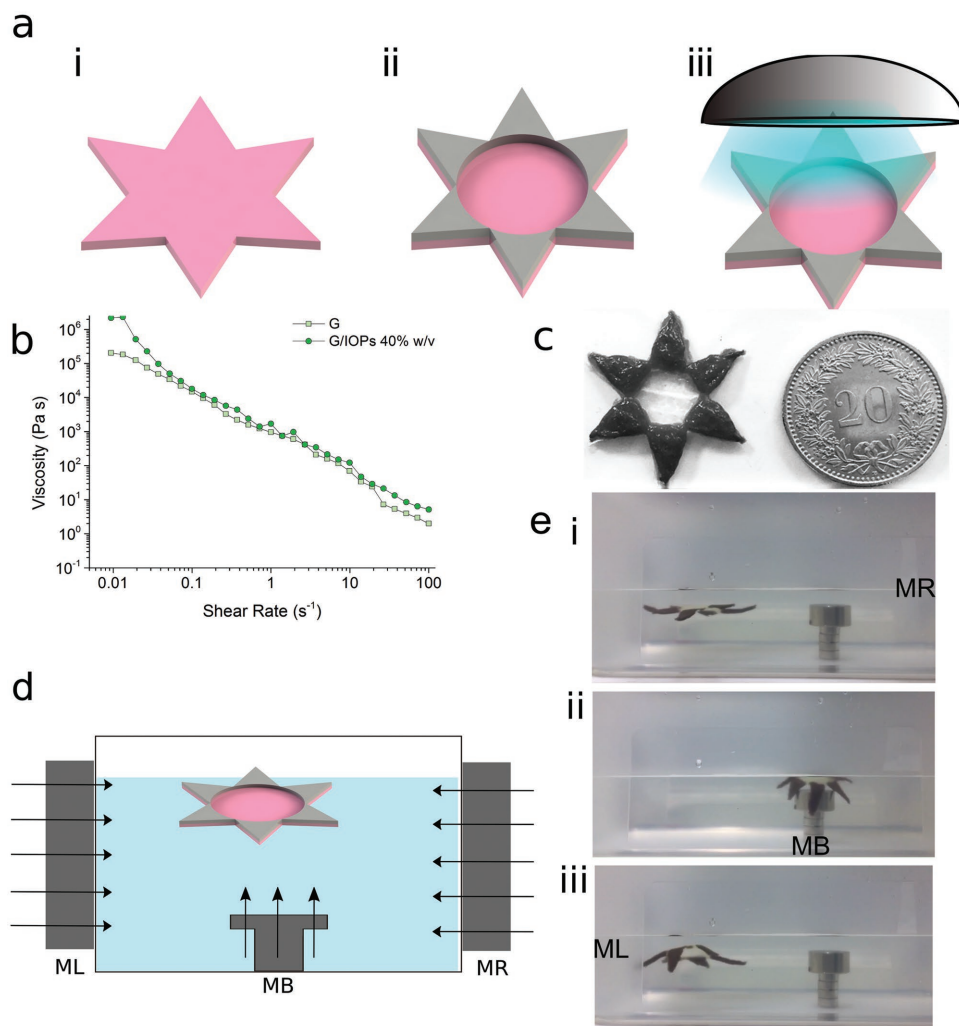


Figure 5. a) Schematic of the process for the fabrication of the 3D-printed starfish. CAD design of the bottom layer of G (i) and the G/IOPs layer 3D-printed on top (ii). The two layers were finally stabilized by means of UV-light exposure (iii). b) Flow behavior of the G and G/IOPs nanocomposite ink. c) 3D-printed structure. d) Schematic representation of remote control of the soft robot motion through on/off switching of three electromagnets. e) Digital image sequence of the starfish soft robot in (i–iii) swimming and (ii) wrapping motion, corresponding to Video S4 in the Supporting Information.

tissue engineering and regeneration, the nanocomposite hydrogels developed in this study can be used as soft mechanical actuators that can respond to spatial and temporally controlled application of magnetic stimulation. Herein, we provide a proof-of-concept of the application of such system to develop a bio-inspired soft robot. In order to create hydrogel constructs that exhibit a controllable motility, anisotropic geometries embedding the nanocomposite elements have to be generated. For this purpose, a key requisite is to ensure the compatibility of our hydrogel as building material for advanced fabrication technologies

that enable accurate 3D spatial orchestration of multiple materials within the same constructs. Recently, the combination of nanotechnologies and 3D printing is revolutionizing approaches to the fabrication of constructs with enhanced multifunctionality.^[39,40] The incorporation of stimuli-responsive cues within living systems enables new avenues for the generation of soft robotics and bionic systems.^[41,42] Within this context, a starfish soft robot was fabricated via 3D printing, as described in **Figure 5a**. First, the printability of the magnetic, temperature- and light-responsive nanocomposite hydrogel was demonstrated,

were stained with Phalloidin (red) and DAPI (blue), respectively. d) Live/Dead assay of C2C12 embedded in the GelMA matrix (G), GelMA doped with IOPs filaments (G/AIOPs), and GelMA doped with a random distribution of IOPs (G/RIOPs) at day 7. A higher number of cells can be noticed by day 7 within the composite material, with $G < G/AIOPs < G/RIOPs$, likely due to a UV screening effect of the PEG-capped iron oxide-based nanoparticles. Scale bar = 100 μm . e) Proliferation of the embedded cells at day 1, 3, and 7 show higher number of cells in G/RIOPs and G/AIOPs than G. f) 2D-FFT analysis of the fluorescent images at day 1, 3, and 7 show alignment of actin and nuclei with the IOPs filament in G/AIOPs. g) Immunofluorescence images of C2C12 cells embedded in G, G/RIOPs, and G/AIOPs cultured in presence (HS+) and absence (HS-) of horse serum at day 11. Myotubes formation is observed in G/AIOPs in the absence of horse serum (-HS). Cells were stained for nuclei (DAPI, blue), actin filaments (Phalloidin, green), and myosin filaments (myosin heavy chain MyHC, orange). Scale bars = 20 μm . * $P < 0.05$, ** $P < 0.01$, one-way ANOVA with a Tukey post hoc test.

and the rheological properties of the magnetic ink were tested and optimized (Figure 5b). After optimization of the nanocomposite gel as printable ink, a star-shaped robot was built as follows: i) printing and partial crosslinking of an initial G hydrogel layer as a foundation; ii) printing of a G/RIOPs layer (40% w/v of IOPs) on top of the previous layer, creating the triangle-shaped fins of the starfish; and iii) additional UV exposure to complete the crosslinking and binding between the two layers. A 3D model slicer (BioCAM, RegenHU, Ltd.) enabled the generation of the bilayered construct for G and G/RIOPs, respectively, and the information was used to instruct an extrusion-based bioprinter (3DDiscovery, RegenHU Ltd.), to print and UV-light crosslink the hydrogels (Figure 5a,c; Video S4, Supporting Information). Anisotropic distribution of the IOPs permitted the locomotion of the robot, when immersed in an aqueous medium: the IOPs-laden fins, flexible as they are composed by a soft gelatin-based hydrogel, perform a flapping movement in response to alternated exposure to magnetic fields. In this particular setup, the robot eventually swims toward the source of the magnetic fields. As shown in the schematic (Figure 5d), three electromagnets have been placed respectively on the left (ML), right (MR), and bottom (MB) of the water pool to guide the starfish navigation by coordinating their on/off switching. As shown in Video S4 in the Supporting Information, by switching on MR, a magnetic field parallel to the water surface was generated, attracting the robot and, at the same time, inducing a swimming motion to the soft robot (Figure 5e). Subsequently, MB was switched on once the soft robot came close to it, while turning off MR. This induced a bending of the IOPs-enriched fins toward MB, that wrapped themselves around it (Figure 5eii) similarly to the mechanism proposed by Gao et al.^[43] More complex coordination of on/off magnetic fields could be studied to control the fins bending for wrapping and flapping motions to generate more intricate trajectories. Finally, the soft robot acquired again the floating position by switching off MB and its motion could be controlled by ML (Figure 5eiii).

3. Conclusion

In conclusion, we reported the synthesis and processing of magnetic nanocomposite hydrogels for the development of anisotropic cell-guidance 3D matrices and for the generation of bioinspired soft robotic systems.

An outstanding functionality of the anisotropic nanocomposite hydrogel was the ability to induce the differentiation of C2C12 skeletal muscle cells in mature myotubes, even in the absence of differentiation medium. This is a fundamental step to create novel biomimetic 3D models and tissue engineering scaffolds, the maturation of which does not rely on external biochemical effectors.

The implementation of additive manufacturing procedures will allow the precise spatial organization of IOPs at the microscale and the generation of patient-specific implantable devices at the macroscale. Overall, these results pave the way to further applications of this multifunctional cytocompatible hydrogel, such as the development of innovative remotely activated mechanotransduction strategies for therapeutic approaches and for the understanding of disease mechanisms.

4. Experimental Section

IOPs Synthesis and Characterization: Synthesis of PEG capped iron oxide-based nanoparticles was carried out according to a coprecipitation and solvothermal method.^[25] Ferric and ferrous chloride at 10^{-1} M and 5×10^{-3} M, respectively, were dissolved in a mixture of diethylene glycol (DEG) and ethylene glycol (EG), in w/w ratio 30:10.^[25] One molar sodium acetate was added and the solution stirred for 3 h at room temperature (RT). 2.5% w/v PEG (MW = 4000 g mol⁻¹) was then added in the case of PEG-capped IOPs and the solution placed in a ventilated oven at 190 °C for 6 h. A dark black precipitate was collected by means of a magnet and washed three times in isopropyl alcohol and three times in ultrapure water Milli-Q grade (with a resistivity of 18.2 MΩ cm at 25 °C). IOPs were imaged via transmission electron microscope JEOL JEM1400 (JEOL Ltd., Tokyo, Japan). TEM was carried out operating at an accelerating voltage of 80 kV with a lanthanum hexaboride (LaB6) source. More in detail, a drop of the nanoparticle suspension for TEM analysis was placed onto carbon-supported copper grids and observed.

X-ray diffraction analysis was carried out on a D-Max/Ultima⁺ diffractometer (Rigaku Corporation, Tokyo, Japan) from 10 to 80°. A CuKα radiation at 30 kV and 100 mA was used as X-ray source and for each measurement the step and the scan speed were of 0.020° and 0.25° min⁻¹, respectively. Raman spectra were acquired on a Horiba XPlora One instrument (Horiba Ltd., Kyoto, Japan) equipped with a continuous Nd-Yag laser with an emission centered at 514.5 nm (with a laser power density of 150 W cm⁻²).

ζ-potential of IOPs and PEG-capped IOPs was measured at room temperature via laser doppler velocimetry using a Zetasizer Nano-ZS90 instrument (Malvern Instruments Ltd., Malvern, UK) and calculated using the Smoluchowski equation.

Synthesis of Methacryloyl Gelatin: Methacryloyl gelatin was synthesized using a previously described method.^[44] A solution 80 mg mL⁻¹ of gelatin in phosphate buffered saline (PBS, 0.01 × 10⁻³ M) was prepared at 60 °C. 1.4 mL methacrylic anhydride was added dropwise into 100 mL of the gelatin solution with vigorous stirring for 3 h. The reaction was stopped with a 5× dilution with preheated PBS. The reaction mixture was dialyzed against demineralized water (with a resistivity 1 MΩ cm) for 6 d at 50 °C using a dialysis membrane (MW cutoff = 12–14 kDa). The solution was then frozen at -20 °C and lyophilized before storage at -20 °C until further use.

IOPs Alignment Kinetics Analysis: The IOPs alignment kinetic was studied placing 1 mL of the G/IOPs mixture in the magnetic field under an inverted optical microscope Axio vert A1 (Carl Zeiss, Oberkochen, Germany). In order to monitor the IOPs filaments growth kinetic, a sequence of images was taken for 30 min every minute. The images were converted to 8-bit, thresholded, and the Feret diameter of the IOPs filaments was measured, using ImageJ 1.51m9 software (NIH, Bethesda, MD). The average IOPs filament length of each time-lapsed picture was calculated, normalized to zero, and plotted versus time. The average filament length of each time-lapsed image was used to obtain the IOPs filaments assembly rate. The obtained curves were fitted with power law functions: <normalized filaments length> = at^b + c, rate of assembly = at^b using Matlab (MathWorks, Natick, MA).^[11] The 2D-FFT pattern was further used to estimate the degree of alignment of the IOPs filaments (Figure S5, Supporting Information), calculating the ratio between the major axis and minor axis of the ellipse that fits the 2D-FFT pattern in each time-lapsed picture.^[40]

Bright-Field Optical Microscopy for Analysis of PEG-IOPs Alignment: The alignment of IOPs was evaluated using a bright-field optical image and analyzed with the 2D-FFT performed with ImageJ software. The pictures were acquired with an EVOS FL auto microscope (ThermoFisher, Waltham, USA). All the images were initially converted to grayscale, and an unsharp mask with a radius of 20–30 pixels was applied. After that, a 2D-FFT was performed on the original images, and the resulting “frequency” domain images were tilted of 90°, to invert the intrinsic rotation due to the 2D-FFT. The pixel intensities were summed along the radius for each angle of the circular projection and plotted as a function of the corresponding angle of acquisition using Oval Profile plugin (authored

by William O'Connell).^[45] For the analysis of the image sequence obtained from a Z-Stack of the hydrogel matrix, an ImageJ macro was written based on the aforementioned methodology and the data obtained were exported and further analyzed with a Python script. In order to avoid differences in sample thickness, camera performance, operator preference for contrast/brightness, and other variables, all the alignment plots were normalized and shifted to a straight baseline of zero.^[45] The fibers diameter distribution was obtained measuring manually the length of the fibers along the minor axis of the elongated IOPs pathways.

Preparation of Anisotropic and Random G/IOPs Nanocomposite Hydrogels: The G/IOPs nanocomposites were prepared at room temperature. 80 mg mL⁻¹ G in PBS solution was obtained at 37 °C with 0.3 mg IOPs and 3 mg photoinitiator (IRGACURE 2959) added per 1 mL. The solution was then vortexed until a homogeneous suspension obtained. Samples with randomly dispersed IOPs or without IOPs were prepared by casting warm suspension and decreasing the temperature for gelation in the absence of external magnetic field. The experimental setup for the fabrication of the anisotropic G/IOPs nanocomposite was based on two NdFeB permanent magnets placed at 5 cm in front of each other on a Teflon support. The Teflon sample holder locates the sample in the middle of the magnetic fields. To self-assemble the IOPs, the warm suspension of G/IOPs was immersed in the static magnetic field with an intensity of 0.02 Tesla for 30 min to trigger IOPs filaments self-assembly along the field lines before cooling down. For the cells embedding, 3 mg of Irigacure, 0.3 mg of IOPs, and 1×10^6 cells were mixed in an 80 mg mL⁻¹ G PBS solution. The cells-laden G and G/RIOPs were prepared as described above, while the cell-laden G/AIOPs nanocomposites were prepared by immersing the warm suspension in the static magnetic field for 30 min. All the samples were then photocrosslinked using a Bio-Link BLX-365 UV radiation chamber (Vilber Lourmat, Collegien, France) for 10 min (0.1 J cm⁻²).

Morphology and Iron Content: Morphological and chemical features of the nanocomposite hydrogels were investigated by scanning electron microscopy and EDX. Morphologic investigation of the G-based samples was carried out by means of a Zeiss EVO scanning electron microscope (Carl Zeiss, Oberkochen, Germany), in variable pressure mode. Gelatin samples were directly positioned onto the sample holder and observed.

Mechanical Tests of the Nanocomposites: Samples of G, G/RIOPs, and G/AIOPs were incubated in PBS to allow equilibrium swelling and stored at 4 °C prior to testing of their mechanical properties with a Dynamic Mechanical Analyzer DMA Q800 (TA Instruments Ltd., the Netherlands). Cylindrical samples of diameter = 6 mm and height = 1 mm were tested under unconfined uniaxial compression ($n = 4$) applying a preload 0.05 N and a force ramp of 0.5 N min⁻¹. For tensile testing ($n = 4$), rectangular strips (30 mm × 5 mm × 0.5 mm), were strained applying a force ramp of 0.05 N min⁻¹. G/AIOPs samples were tested with the tensile stress applied in the direction parallel to that of the preferential IOPs orientation. For both compression and tensile tests, the tangent modulus was calculated as the slope of the linear region between 10% and 15% deformation (Figure S12, Supporting Information). Local compression properties of the samples immersed in PBS were assessed using a nanoindenter (Piuma, Optics 11, the Netherlands), equipped with a spherical tip probe (cantilever stiffness = 0.42 N m⁻¹, tip diameter = 44 μm). For each individual measurement, the tip was brought to contact with the surface and held in place for 2 s, prior to the initiation of the test. Subsequently, an 18 μm strain was applied on the sample during 1 s and the achieved deformation was held for 7 s. After this relaxation time, the hydrogel was slowly unloaded during 20 s. For each sample, five regions of 100 μm² were randomly selected on the hydrogel surface and each area was probed in five equally distanced spots. The effective elastic modulus was calculated using the slope of the initial portion of the unloading curve using the Oliver–Pharr theory as previously described.^[46]

Cell Isolation and Culture: Bone marrow aspirates were obtained with informed consent from patients and with full approval from the Ethics Committee of the University of Freiburg Medical Centre (EK-Freiburg: 135/14). hMSCs (1st donor: male, 65 years old; 2nd donor: female, 73 years old) were isolated from bone marrow aspirates and cultured

according to established protocol.^[47] Minimum Essential Medium alpha (α-MEM supplemented with 10% Sera Plus bovine serum, 100 U mL⁻¹ Penicillin and 100 μg mL⁻¹ Streptomycin and 5 ng mL⁻¹ recombinant FGFb) was used for both isolation and expansion of hMSCs. Cultures were maintained at 37 °C in humidified atmosphere of 5% CO₂ with media change every second day.^[47] hMSCs were seeded at passage 3 on the surface of G, G/RIOPs, and G/AIOPs at a density of 1×10^6 cells mL⁻¹.

Statistical Analysis: Quantitative results were expressed as mean ± standard deviation (SD), and the statistical analyses were performed using the GraphPad Prism 6.0 software package (GraphPad Software, USA). Comparisons between the experimental groups were performed with a one-way ANOVA, with a Tukey post hoc test. A statistical significance was defined * $P < 0.05$, ** $P < 0.01$.

Cell Staining: Actin organization of hMSCs seeded on nanocomposite surfaces was observed at 4, 24, and 72 h after seeding using Phalloidin staining. At each time point, samples were washed in PBS, fixed in buffered 4% formalin solution for 20 min at RT, and permeabilized with 0.25% Triton X-100 for 20 min at RT. Actin filaments were stained with Phalloidin-TRITC (2×10^{-6} M) for 45 min at RT. Samples were then washed with PBS and stained with DAPI (500×10^{-9} M) for 10 min. Samples were imaged using EVOS2 FL auto cell imaging system (ThermoFisher, Waltham, USA).

C2C12 Embedded in the Nanocomposites: C2C12 myoblasts (American Type Culture Collection) were maintained at low density in Dulbecco's Modified Essential Medium (DMEM) with 4.5 g L⁻¹ glucose supplemented with 10% v/v fetal bovine serum (FBS) and passaged every second day. C2C12 were embedded in G, G/RIOPs, and G/AIOPs at a density of 1×10^6 cells mL⁻¹ of hydrogel. To induce myoblast differentiation, samples were first cultured in DMEM 4.5 g L⁻¹ glucose supplemented with 10% FBS until cells within the hydrogels reached 85–90% confluence and then washed in PBS and cultured in differentiation medium (DMEM 4.5 g L⁻¹ supplemented with 2% v/v HS) for 4 d. During the differentiation period, media was changed every 24 h. At day 1, 3, and 6 of culture, samples were washed in PBS, fixed in buffered 4% formalin solution for 20 min at RT, and permeabilized with 0.25% Triton X-100 for 20 min at RT. Actin filaments were stained with Phalloidin-TRITC (2×10^{-6} M) for 45 min at RT. Samples were then washed with PBS and stained with DAPI (500×10^{-9} M) for 10 min. Samples were imaged using EVOS2 FL auto cell imaging system (ThermoFisher, Waltham, USA). The formation of myotubes was assessed by MyHC immunofluorescent staining after 4 d of differentiation. After permeabilization, samples were incubated ON at 4 °C in permeabilization solution containing primary mouse MyHC antibody (1:400 dilution). Samples were incubated for 2 h at RT in permeabilization solution containing AF555 anti mouse antibody (1:500 dilution). Actin filaments and nuclei were stained with Phalloidin-FITC and DAPI, respectively, as previously described. Samples were imaged using an LSM510 confocal microscope (Carl Zeiss, Oberkochen, Germany).

Live and Dead Assay: A Live and Dead assay was performed at day 7. A staining solution containing 10×10^{-6} M Calcein-AM and 5×10^{-6} M Ethidium homodimer-1 was prepared in serum free DMEM 4.5 g L⁻¹ glucose. Cell-laden hydrogels were washed three times in PBS and then transferred to staining solution for 1 h at 37 °C. The samples were then washed three times in PBS and imaged using an LSM510 confocal microscope (Carl Zeiss, Germany).

Nuclei Number Quantification: The nuclei were counted using the particles analyze function of ImageJ software thresholding the blue channel of the original images performing the same operation on three different images.

Ink Rheology: For the analysis of the flow behavior, a PBS solution of G (15% w/v) was prepared and subsequently the IOPs (40% w/v) were mixed with the G prepolymer mixture. The flow behavior was investigated with the Anton-Paar MCR-302 rheometer, by rotational measurement, in shear rate interval (0.01–100 s⁻¹), with a parallel geometry PP-25 and a gap size 0.4 mm, at 25 °C.

Magnetic Soft Robot 3D Printing Protocol: The 3D printing of soft robot using G/RIOPs and G ink was carried out with a 3D Discovery instrument (RegenHU Ltd), using FreeCad (J Riegel, W Mayer, Y van

Havre, Version 0.16.6706) program and MMconverter (RegenHU, Ltd.) to design and slice the printed architectures. The printing process was done in a temperature range between 25 and 30 °C, using a 4 bar pressure, and Teflon covered needle (0.3 mm inner diameter). The 3D-printed G/IOPs hydrogel was photopolymerized in the previously described UV light curing system excitation for 10 min (0.1 J cm⁻²).

Supporting Information

Supporting Information is available from the Wiley Online Library or from the author.

Acknowledgements

The authors would like to thank Mr. Flavio Linardi for technical support, and Dr. Keith Thompson and Dr. Elena Della Bella for critical review of the manuscript.

Conflict of Interest

The authors declare no conflict of interest.

Keywords

biofabrication, cell guidance, magnetic assembly, soft robotics, stimuli-responsive hydrogel

Received: July 6, 2018

Revised: November 7, 2018

Published online: December 18, 2018

- [1] T. Mammoto, D. E. Ingber, *Development* **2010**, *137*, 1407.
- [2] M. Théry, V. Racine, A. Pépin, M. Piel, Y. Chen, J.-B. Sibarita, M. Bornens, *Nat. Cell Biol.* **2005**, *7*, 947.
- [3] S. R. Shin, B. Migliori, B. Miccoli, Y. C. Li, P. Mostafalu, J. Seo, S. Mandla, A. Enrico, S. Antona, R. Sabarish, T. Zheng, L. Pirrami, K. Zhang, Y. S. Zhang, K. Tak Wan, D. Demarchi, M. R. Dokmeci, A. Khademhosseini, *Adv. Mater.* **2018**, *30*, <https://doi.org/10.1002/adma.201704189>.
- [4] W. Hu, G. Z. Lum, M. Mastrangeli, M. Sitti, *Nature* **2018**, *554*, 81.
- [5] L. Ionov, *Mater. Today* **2014**, *17*, 494.
- [6] H. Priya James, R. John, A. Alex, K. R. Anoop, *Acta Pharm. Sin. B* **2014**, *4*, 120.
- [7] A. Sydney Gladman, E. A. Matsumoto, R. G. Nuzzo, L. Mahadevan, J. A. Lewis, *Nat. Mater.* **2016**, *15*, 413.
- [8] W.-G. Bae, J. Kim, Y.-H. Choung, Y. Chung, K. Y. Suh, C. Pang, J. H. Chung, H. E. Jeong, *Biomaterials* **2015**, *69*, 158.
- [9] B. Bharti, O. D. Velev, *Langmuir* **2015**, *31*, 7897.
- [10] Y. Li, G. Huang, X. Zhang, B. Li, Y. Chen, T. Lu, T. J. Lu, F. Xu, *Adv. Funct. Mater.* **2013**, *23*, 660.
- [11] B. Bharti, A.-L. Fameau, O. D. Velev, *Faraday Discuss.* **2015**, *181*, 437.
- [12] K. Hu, J. Sun, Z. Guo, P. Wang, Q. Chen, M. Ma, N. Gu, *Adv. Mater.* **2015**, *27*, 2507.
- [13] S. Bettini, G. Giancane, R. Pagano, V. Bonfrate, L. Salvatore, M. Madaghiele, A. Buccolieri, D. Manno, A. Serra, G. Maruccio, A. G. Monteduro, Z. Syrgiannis, L. Valli, M. Prato, *J. Mater. Chem. B* **2017**, *5*, 7547.
- [14] Y. Bao, J. A. Sherwood, Z. Sun, *J. Mater. Chem. C* **2018**, *6*, 1280.
- [15] W. Wu, C. Z. Jiang, V. A. L. Roy, *Nanoscale* **2016**, *8*, 19421.
- [16] A. Omidinia-Anarkoli, S. Boesveld, U. Tuvshindorj, J. C. Rose, T. Haraszti, L. De Laporte, *Small* **2017**, *13*, 1.
- [17] K. Yue, G. Trujillo-de Santiago, M. M. Alvarez, A. Tamayol, N. Annabi, A. Khademhosseini, *Biomaterials* **2015**, *73*, 254.
- [18] J. Ramón-Azcón, S. Ahadian, M. Estili, X. Liang, S. Ostrovidov, H. Kaji, H. Shiku, M. Ramalingam, K. Nakajima, Y. Sakka, A. Khademhosseini, T. Matsue, *Adv. Mater.* **2013**, *25*, 4028.
- [19] S. Ahadian, J. Ramón-Azcón, M. Estili, X. Liang, S. Ostrovidov, H. Shiku, M. Ramalingam, K. Nakajima, Y. Sakka, H. Bae, T. Matsue, A. Khademhosseini, *Sci. Rep.* **2014**, *4*, 1.
- [20] N. Abd Rahman, F. Ibrahim, B. Yafouz, *Sensors (Basel)* **2017**, *17*, E449.
- [21] S. Lanone, P. Andujar, A. Kermanizadeh, J. Boczkowski, *Adv. Drug Delivery Rev.* **2013**, *65*, 2063.
- [22] M. M. Schmauch, S. R. Mishra, B. A. Evans, O. D. Velev, J. B. Tracy, *ACS Appl. Mater. Interfaces* **2017**, *9*, 11895.
- [23] A. Ghosh, C. Yoon, F. Ongaro, S. Scheggi, F. M. Selaru, S. Misra, D. H. Gracias, *Front. Mech. Eng.* **2017**, *3*, 7.
- [24] C.-M. Horejs, *Nat. Rev. Mater.* **2018**, *3*, 18007.
- [25] V. Bonfrate, D. Manno, A. Serra, L. Salvatore, A. Sannino, A. Buccolieri, T. Serra, G. Giancane, *J. Colloid Interface Sci.* **2017**, *501*, 185.
- [26] B. Bharti, A.-L. Fameau, M. Rubinstein, O. D. Velev, *Nat. Mater.* **2015**, *14*, 1104.
- [27] J. Lim, C. Lanni, E. R. Evarts, F. Lanni, R. D. Tilton, S. A. Majetich, *ACS Nano* **2011**, *5*, 217.
- [28] E. M. Purcell, *Am. J. Phys.* **1977**, *45*, 3.
- [29] P. Lin, T. Zhang, X. Wang, B. Yu, F. Zhou, *Small* **2016**, *12*, 4386.
- [30] Z. Zhao, R. Fang, Q. Rong, M. Liu, *Adv. Mater.* **2017**, *29*, 1703045.
- [31] J. Kim, J. R. Staunton, K. Tanner, *Adv. Mater.* **2016**, *28*, 132.
- [32] J. C. Rose, M. Cámara-Torres, K. Rahimi, J. Köhler, M. Möller, L. De Laporte, *Nano Lett.* **2017**, *17*, 3782.
- [33] Z. Guo, K. Hu, J. Sun, T. Zhang, Q. Zhang, L. Song, X. Zhang, N. Gu, *ACS Appl. Mater. Interfaces* **2014**, *6*, 10963.
- [34] W. P. Daley, K. M. Yamada, *Curr. Opin. Genet. Dev.* **2013**, *23*, 408.
- [35] C.-P. Heisenberg, Y. Bellaïche, *Cell* **2013**, *153*, 948.
- [36] B. D. Fairbanks, M. P. Schwartz, C. N. Bowman, K. S. Anseth, *Biomaterials* **2009**, *30*, 6702.
- [37] K. S. Lim, R. Levato, P. F. Costa, M. D. Castilho, C. R. Alcalá-Orozco, K. M. A. van Dorenmalen, F. P. W. Melchels, D. Gawlitza, G. J. Hooper, J. Malda, T. B. F. Woodfield, *Biofabrication* **2018**, *10*, 034101.
- [38] D. Petta, A. R. Armiento, D. Grijpma, M. Alini, D. Eglin, M. D'Este, *Biofabrication* **2018**, *10*, 044104.
- [39] R. D. Farahani, M. Dubé, D. Therriault, *Adv. Mater.* **2016**, *28*, 5794.
- [40] D. Kokkinis, M. Schaffner, A. R. Studart, *Nat. Commun.* **2015**, *6*, 8643.
- [41] Y. L. Kong, M. K. Gupta, B. N. Johnson, M. C. McAlpine, *Nano Today* **2016**, *11*, 330.
- [42] M. Schaffner, J. A. Faber, L. Pianegonda, P. A. Rühls, F. Coulter, A. R. Studart, *Nat. Commun.* **2018**, *9*, 878.
- [43] W. Gao, L. Wang, X. Wang, H. Liu, *ACS Appl. Mater. Interfaces* **2016**, *8*, 14182.
- [44] J. W. Nichol, S. T. Koshy, H. Bae, C. M. Hwang, S. Yamanlar, A. Khademhosseini, *Biomaterials* **2010**, *31*, 5536.
- [45] C. E. Ayres, B. S. Jha, H. Meredith, J. R. Bowman, G. L. Bowlin, S. C. Henderson, D. G. Simpson, *J. Biomater. Sci., Polym. Ed.* **2008**, *19*, 603.
- [46] P. R. Moshtagh, B. Pouran, N. M. Korthagen, A. A. Zadpoor, H. Weinans, *J. Biomech.* **2016**, *49*, 3602.
- [47] O. F. W. Gardner, M. Alini, M. J. Stoddart, *Methods Mol. Biol. (Clifton, N.J.)* **2015**, *1340*, 41.